Applied Catalysis B: Environmental 181 (2016) 371–378

Contents lists available at ScienceDirect

Applied Catalysis B: Environmental

journal homepage: www.elsevier.com/locate/apcatb

Green synthesis of Pt–Au dendrimer-like nanoparticles supported on polydopamine-functionalized graphene and their high performance toward 4- nitrophenol reduction

Weichun Ye[a,b,*], Jing Yu[a], Yaxin Zhou[a], Daqiang Gao[b], Daoai Wang[c], Chunming Wang[a], Desheng Xue[b,*]

[a] State Key Laboratory of Applied Organic Chemistry and Department of Chemistry, Lanzhou University, Lanzhou 730000, China
[b] Key Laboratory for Magnetism and Magnetic Materials of MOE and Department of Physics, Lanzhou University, Lanzhou 730000, China
[c] State Key Laboratory of Solid Lubrication, Lanzhou Institute of Chemical Physics, Chinese Academy of Sciences, Lanzhou 730000, China

ARTICLE INFO

Article history:
Received 4 May 2015
Received in revised form 3 August 2015
Accepted 5 August 2015
Available online 10 August 2015

Keywords:
Reduced graphene oxide
Polydopamine
Pt–Au alloy
Dendrimer-like
4-Nitrophenol reduction

ABSTRACT

A facile, environmentally friendly route is demonstrated for the synthesis of Pt–Au dendrimer-like nanoparticles on the surface of polydopamine (PDA)-wrapped reduced graphene oxide (RGO), in which Pt–Au alloy nanoparticles are synthesized by the reduction of H_2PtCl_6 and $HAuCl_4$ with ascorbic acid. The effects of support material and chemical composition on the catalytic activity for the reduction of 4-nitrophenol (4-NP) are investigated in detail. Pt nanoparticles supported on PDA/RGO (Pt-PDA/RGO) exhibit significantly higher catalytic activity as compared to those exhibited by Pt nanoparticles deposited on pristine graphene sheets (Pt-RGO) and commercial Pt/C catalyst. Furthermore, the chemical composition seriously affects the catalytic ability of the catalysts. With Pt-to-Au molar ratios of 3/1 and 1/1, significantly enhanced catalytic activities are observed, outperforming the support decorated with each single constituent. The high activity of Pt-Au-PDA/RGO can be explained by electronic effect involving in two types of electron transfers: (1) from the PDA coating to both Au and Pt atoms; (2) from Au to Pt atoms. Moreover, the Pt3Au1-PDA/RGO composite keeps a stable conversion efficiency of around 100% over six successive reduction reaction cycles. Through an experimental device of "filtering and catalyzing," the Pt3Au1- PDA/RGO sample exhibits superior efficiency for the purification of water containing 4-NP. Within 8 s, the water becomes colorless.

© 2015 Elsevier B.V. All rights reserved.

1. Introduction

Noble metal nanoparticles have attracted considerable attention caused by their distinctive physicochemical properties and their potential applications as a new class of efficient catalysts [1–5]. However, the incorporation of multiple metals, as compared to a single metal, into a single system is more advantageous for most applications, caused by a synergistic effect [6–12]. For example, platinum–gold nanoparticles have been used as catalysts for reactions such as NO reduction [6], CO oxidation [7], glycerol oxidation [8], and nitrophenol reduction [9–14].

Furthermore, for maximizing the catalytic activity of metal nanoparticles, a suitable carbon support is required for their dispersion [15,16]. Compared to conventional carbon materials including carbon black and carbon nanotubes, graphene or reduced graphene oxide (RGO) is a promising candidate as a new 2D support with high surface area and excellent electrical properties [17–19]. Generally, graphene is mostly prepared by the chemical reduction of graphene oxide (GO), which is obtained by the chemical oxidation of graphite. Similarly, this chemical reduction is favorable for the fabrication of metal nanoparticle–graphene composites. However, the reductants used for the chemical reduction of GO and of metal ions are usually hydrazine or sodium borohydride ($NaBH_4$), each of which is highly toxic. Thus, a facile, environmentally friendly approach for effectively producing metal nanoparticle/graphene hybrids needs to be explored. In addition, RGO exhibits hydrophobicity, which limits its catalytic performance to heterogeneous catalysis. To solve this fundamental problem, a transition layer, polydopamine (PDA), is introduced, which exhibits good biocompatibility and stability. Also, PDA can be easily introduced by the self-polymerization of dopamine at weakly alkaline pH [20–22]. Importantly, dopamine is an eco-friendly reducing agent for the reduction of GO [23–29].

* Corresponding authors at: Key Laboratory for Magnetism and Magnetic Materials of MOE and Department of Physics, Lanzhou University, Lanzhou 730000, China.
E-mail addresses: yewch@lzu.edu.cn (W. Ye), xueds@lzu.edu.cn (D. Xue).

http://dx.doi.org/10.1016/j.apcatb.2015.08.013
0926-3373/© 2015 Elsevier B.V. All rights reserved.

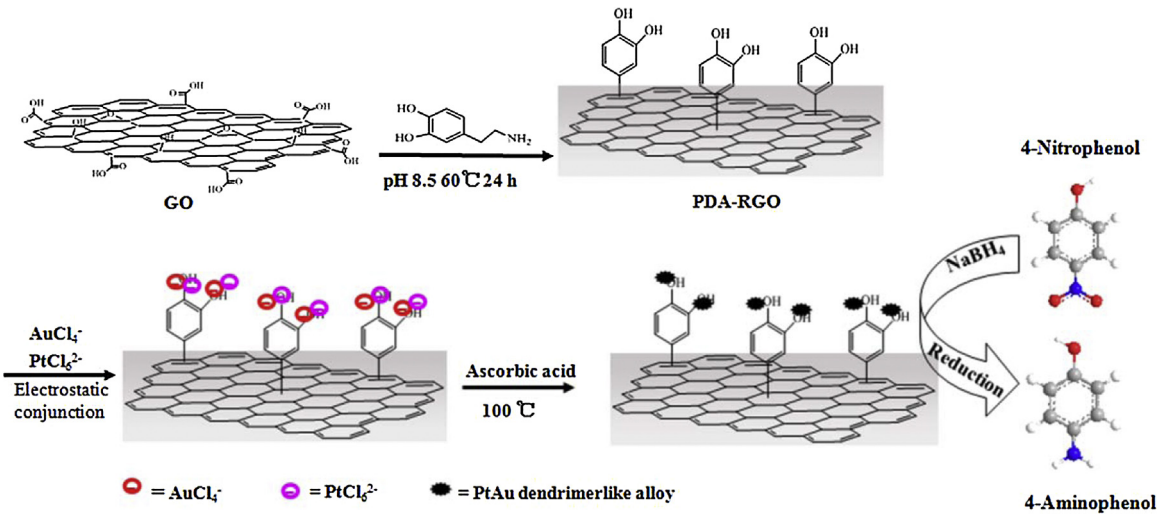

Scheme 1. Synthetic scheme of Pt–Au dendrimer-like alloy nanoparticles supported on PDA/RGO for the efficient reduction of 4-nitrophenol.

In this study, we report highly active Pt–Au dendrimer-like alloy nanoparticles supported on the surface of PDA/RGO, where PDA acting as a biopolymer was used to achieve the reduction and simultaneous functionalization of RGO, and Pt–Au dendrimer-like alloy nanoparticles were obtained via the *in situ* reduction of their metal precursors by an aqueous ascorbic acid solution. The whole process of our experiment followed the concept of green chemistry. The catalytic activity and stability of Pt–Au nanoparticles supported on PDA/RGO were estimated for the reduction of 4-nitrophenol (4-NP) as a model reaction. The effects of support material and chemical composition of Pt–Au nanoparticles on the catalytic performance were discussed in detail. Finally, Pt–Au nanoparticles supported on PDA/RGO exhibited excellent efficiency for purifying 4-NP- contaminated water.

2. Experimental

2.1. Materials

GO was purchased from Nanjing XFNANO Tech Co., Ltd. $HAuCl_4$, H_2PtCl_6, ascorbic acid, and 4-NP were purchased from Beijing Chemical Factory (Beijing, China) and used as received without further purification. Dopamine was purchased from Aldrich. A Pt/C catalyst (10 wt% of Pt loading) was commercially obtained. Water used in all experiments was purified using a Millipore system.

2.2. Characterization

High-resolution transmission electron microscopy (HRTEM) images were recorded on a transmission electron microscope (TEM, Tecnai G2 F30, FEI, USA). The samples for TEM were prepared by placing a drop of the as-prepared solution on carbon-coated copper grids followed by drying. X-ray photoelectron spectroscopy (XPS) measurements were performed on a multifunctional spectrometer (Thermo Scientific) using Al Kα radiation. An X-ray diffraction analyzer (XRD, Rigaku D/max-2400, Cu K-Alpha radiation, $\lambda = 0.1541$ nm) was used. UV–vis spectra were recorded on a UV–vis 800 spectrophotometer at room temperature.

2.3. Synthesis of Pt–Au-PDA/RGO

The synthesis of Pt–Au dendrimer-like alloy nanoparticles on PDA/RGO sheets was carried out in two steps: first, PDA/RGO was prepared according to our previous study [28,29]. Briefly, 10 mg of GO was dispersed into 20 mL of a Tris-HCl (10 mM, pH 8.5) solution. Subsequently, 10 mg of dopamine hydrochloride was added, and the mixture was stirred at 60 °C for 24 h. The dark brown suspension turned into a black solution. The products were collected by centrifugation and thoroughly rinsed with water. Next, the obtained PDA/RGO was re-dispersed into 40 mL water. Then, 0.5 mL of aqueous solutions of $HAuCl_4$ and H_2PtCl_6 were added dropwise to the PDA/RGO solution. The mixture solution was heated to boiling under stirring. Finally, 1 mL of 0.1 M ascorbic acid was subsequently added to the boiling solution. After 30 min, the Pt–Au nanoparticles were obtained on PDA/RGO, termed as Pt–Au-PDA/RGO. The total concentration of chloroplatinic acid and chloroauric acid was maintained at 10 mM, and the molar ratios of chloroplatinic acid and chloroauric acid were adjusted at 4/0, 3/1, 1/1 and 0/4. These samples were termed as Pt-PDA/RGO, Pt3Au1-PDA/RGO, Pt1Au1-PDA/RGO, and Au-PDA/RGO, respectively.

For comparison, Pt-RGO composites were synthesized by the deposition of Pt or Pt–Au (1:1 of molar ratio) nanocrystals on RGO sheets by the reduction of $NaBH_4$ without PDA modification under the same procedure, termed as Pt-RGO or Pt1Au1-RGO, respectively.

2.4. Catalytic reduction of 4-NP

Experiments for the reduction of 4-NP were carried out at room temperature in a standard quartz cell with a path length of 1 cm. The aqueous solution of $NaBH_4$ (0.1 M) was freshly prepared. First, 0.3 mL of a $NaBH_4$ solution was mixed with 2.7 mL of 0.1 mM 4-NP in the quartz cell. Then, 30 μL of the samples (2 mg/mL) was added in the mixture. Immediately after that, the UV–vis absorption spectra were recorded with a time interval at a scanning range of 250–500 nm at room temperature.

The reusability of Pt3Au1-PDA/RGO was measured by six successive repeated cycles of the reduction of 4-NP. After 5 min of reaction, the reaction solution was collected by centrifugation before measuring the absorbance at 400 nm. The recycled catalyst was washed several times with deionized water and was reused for the next cycle.

3. Results and discussion

3.1. Characterization of Pt–Au nanoparticles supported on PDA/RGO

The PDA layer is not only a biopolymer with good biocompatibility, but also has abundant amine and catechol groups, which

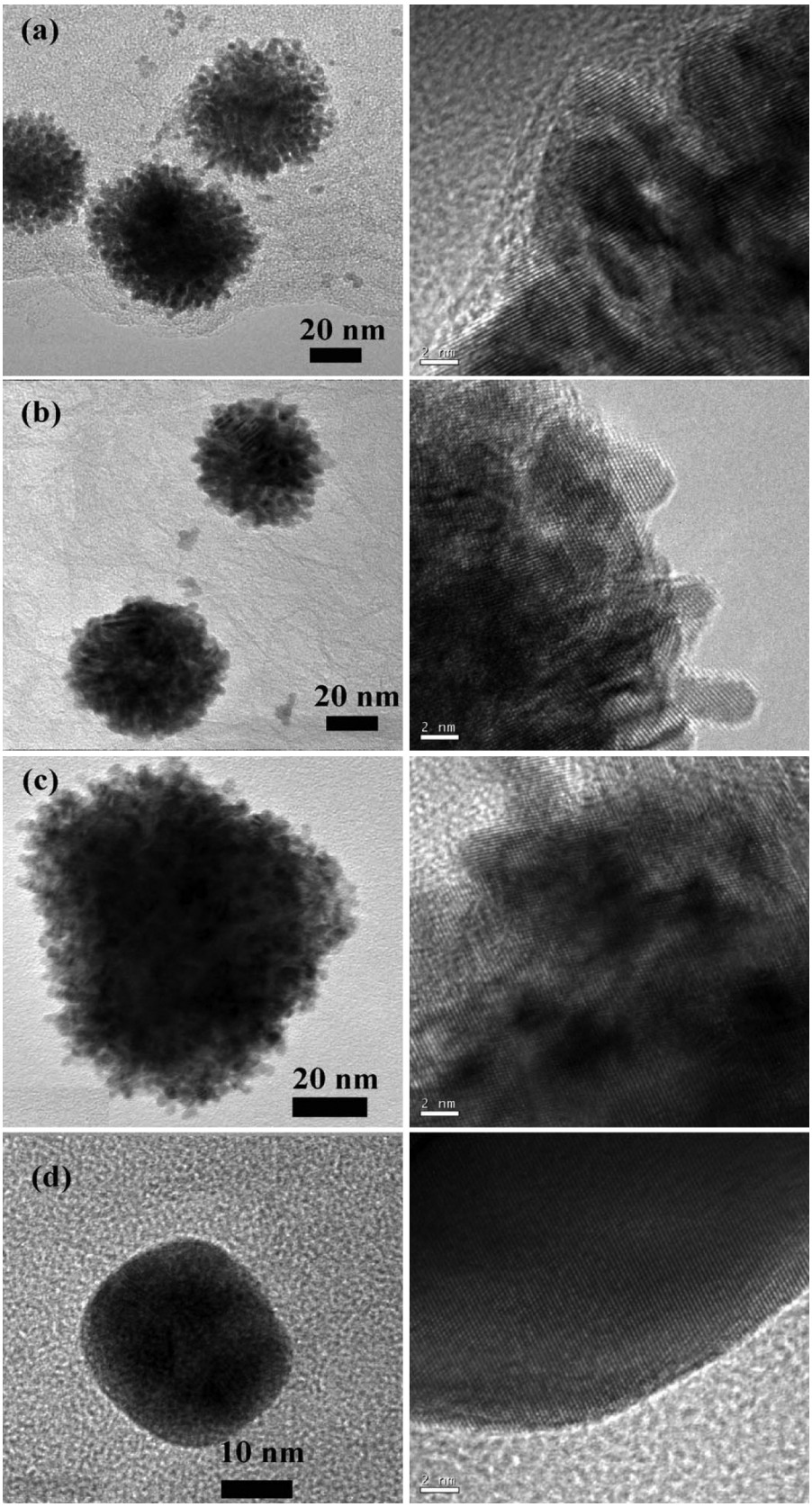

Fig. 1. TEM (left) and HRTEM (right) images of (a) Pt-PDA/RGO, (b) Pt3Au1-PDA/RGO, (c) Pt1Au1-PDA/RGO, and (d) Au-PDA/RGO.

help in the stabilization of metal nanoparticles [22]. In our previous study [28,29], we have found that the multifunctional biopolymer plays dual roles of dispersing stable RGO into an aqueous solution and providing functional groups to bind metal ions and metal nanoparticles. As seen in Scheme 1, PDA/RGO was first synthesized by the reduction and self-polymerization of dopamine. Then, the amine and catechol groups as preferential reactive sites were in electrostatic conjunction with $PtCl_6^{2-}$ and $AuCl_4^-$, followed by the reduction of ascorbic acid to produce Pt–Au-PDA/RGO composites.

First, we investigated the effect of PDA modification on the morphology of platinum nanoparticles. As shown in the TEM image of Pt-PDA/RGO, platinum nanoparticles exhibited dendrimer nanostructures, which were assembled with small spherical nanoparticles of a diameter of 2.7 nm (Fig. 1A). As can be observed in the TEM images, these Pt dendrimer-like nanoparticles were uniformly dispersed on graphene nanosheets (Fig. S1a and b). For comparison, the reduction of $NaBH_4$ and no modification of PDA led to the formation of spherical nanoparticles with a diameter of 6 nm (Fig. S2). Also, the spherical nanoparticles were easily aggregated together (Fig. S2a and b).

Fig. 1 also shows the morphological evolution of the Pt–Au nanoparticles with the variation of Pt-to-Au ratios. Except for Au-PDA/RGO demonstrating large spherical nanoparticles with a diameter of 26 nm, Pt–Au alloys exhibited a dendrimer-like nanostructure composed of small nanoparticles. The dendrimer-like nanostructure has rich edges and corner atoms, which are important for the enhancement of their catalytic activity [30]. As shown in the HRTEM images of the Pt–Au alloy nanoparticles on PDA/RGO with different chemical compositions (right images of Fig. 1), there was no indication of a core–shell structure [31]. The crystal lattice was clearly observed in the entire nanoparticle for all Pt–Au systems with about 2.3 Å of lattice fringes, which is assigned to the (1 1 1) crystal plane of the face-centered cubic (fcc) crystalline structure.

Obviously, the amine and catechol groups of PDA molecules played an important role in the formation of small and well-dispersed Pt–Au alloy nanoparticles by the electrostatic conjunction of the negatively charged ions ($PtCl_6^{2-}$ and $AuCl_4^-$).

Fig. S3 shows the UV–vis spectra of the Pt–Au-PDA/RGO hybrids with different chemical composition. A characteristic surface plasmon resonance (SPR) peak at approximately 550 nm was clearly observed for monometallic Au-PDA/RGO. As Au was alloyed with Pt (for Pt3Au1-PDA/RGO and Pt1Au1-PDA/RGO), the Au SPR peak was suppressed and appeared at a lower wavelength (~540 nm). For monometallic Pt modified on PDA/RGO, no visible absorption was observed.

Fig. 2 shows the XRD patterns of PDA/RGO supported with bimetallic and monometallic nanoparticles. Each pattern exhibited an fcc structure feature with (1 1 1), (2 0 0), (2 2 0), and (3 1 1) faces, except for a typical diffraction peak (0 0 2) of RGO. Each face demonstrated a single peak irrespective of a single metal or a bimetal, and the peaks for the bimetal nanoparticles were intermediate between the corresponding peaks of Au and Pt. The XRD results suggest that Pt–Au nanoparticles demonstrate an alloy structure. According to Vegard's law [32], the lattice constant (d) can be calculated, and Table 1 lists the d values. The d values of the Pt–Au bimetallic nanoparticles were in between those of monometallic Au (0.407 nm) and Pt (0.388 nm); they also linearly decreased with increasing Pt mole fraction in the electrolyte, as shown in the inset of Fig. 2. This result indicates an alloy feature in which Pt and Au are tightly mixed together [33]. By contrast, as pure RGO was used as the support for the simultaneous deposition of Pt and Au, the XRD pattern of the corresponding composite (Pt1Au1-RGO, Fig. S4) exhibited two sets of diffraction reflections (Pt and Au), which indicates the phase-segregation state of Pt and Au [34].

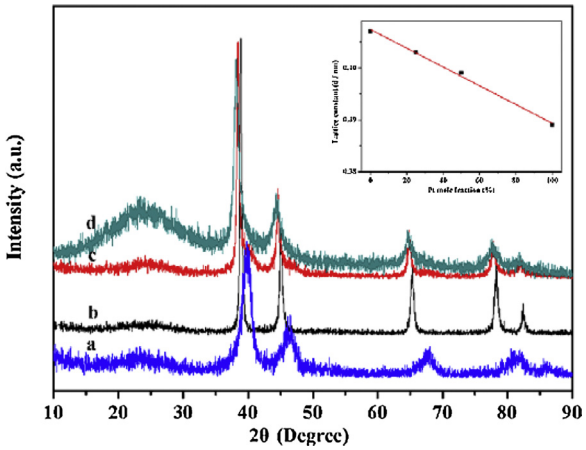

Fig. 2. XRD patterns of (a) Pt-PDA/RGO, (b) Pt3Au1-PDA/RGO, (c) Pt1Au1-PDA/RGO, and (d) Au-PDA/RGO. The inset shows the plot of lattice constant (d) vs. Pt mole fraction.

Fig. 3 shows the XPS spectra of Au 4f (A) and Pt 4f (B) regions for these samples. Each Pt–Au-based sample exhibited four energy bands, which are assigned to metallic Pt $4f_{7/2}$, Pt $4f_{5/2}$, Au $4f_{7/2}$, and Pt $4f_{5/2}$, respectively. Furthermore, the Au 4f binding energies (BEs) shifted to a lower peak value for Pt–Au alloy nanoparticles, as compared to monometallic Au nanoparticles. The same negative shifts also appeared in the Pt 4f regions for Pt–Au alloy nanoparticles as compared to monometallic Pt nanoparticles. These large negative shifts in both Au 4f and Pt 4f in Pt–Au alloy nanoparticles suggest that a negative charge is loaded on Pt–Au alloys [35]. As reported in the literature [36,37], the electron donated from the stabilizer (*e.g.*, poly(vinylpyrrolidone)) to a metal like Pt and Au leads to a negative shift of the BE in the XPS spectra. Hereby, we can suppose that the large negative shifts in both Pt 4f and Au 4f are due to electron donation from the PDA coating and the interaction between Pt–Au alloys and the PDA coating.

3.2. Effect of supported material on catalyzed reduction of 4-NP

Here, we selected the reduction of 4-NP to 4-AP as a model for testing the catalytic activity of Pt–Au-PDA/RGO hybrids. The reaction process was monitored by UV–vis spectroscopy. The reduction of 4-NP by $NaBH_4$ is thermodynamically favorable because the difference of their standard electrode potentials is greater than zero ($\Delta E^0 = E^0_{(4\text{-NP/4-NAP})} - E^0_{(H3BO3/BH4)} = -0.76 - (-1.33) = 0.67$ V) [38]; however, this reaction was kinetically restricted in the absence of an efficient catalyst. By adding $NaBH_4$ into a 4-NP solution, the solution changed from light yellow to bright yellow, caused by the formation of 4-nitrophenolate ions under highly basic conditions. The original absorption peak also shifted from 317 nm to 400 nm [39] (Fig. S5).

Noble metal nanoparticles are vital to catalyze the reduction of 4-NP by $NaBH_4$. A controlled experiment was first performed. As PDA/RGO was added into the reduction mixture, the absorption peak at 400 nm slowly decreased with reaction time, as shown in Fig. S6. Nonetheless, the peak at 300 nm corresponding to the product 4-aminophenol (4-AP) [40] was not observed even after 30 min. This indicates that the decreased intensity of the peak at 400 nm results from the adsorption of 4-NP rather than from the catalysis by PDA/RGO. Conversely, as the catalyst contained Pt nanoparticles, the intensity of the absorption peak at 400 nm gradually decreased with increasing reaction time (Fig. S7a). In the meantime, a new absorption peak corresponding to 4-AP appeared at 300 nm. However, we noticed that its successive intensity did not increase in sequence, similar to the previous reports [11,41]. It can

Table 1
Comparison of the normalized rate constants (k_{nor}) and TOF of the catalysts for the reduction of 4-NP with $NaBH_4$.

Catalyst	c (4-NP) [a] (mM)	c (Pt or Au) (mM)	k_{app} [b] ($\times 10^{-3}$ s^{-1})	TOF (h^{-1}) [c]
Commerical Pt/C catalyst	0.1	0.01	0.37	8
Pt-RGO	0.1	0.01	0.95	20
Pt1Au1-RGO	0.1	0.01	0.69	14
Pt-PDA/RGO	0.1	0.01	3.43	72
Pt3Au1-PDA/RGO	0.1	0.01	9.58	200
Pt1Au1-PDA/RGO	0.1	0.01	5.67	118
Au-PDA/RGO	0.1	0.01	2.00	42

[a] c: concentration.
[b] k_{app}: apparent rate constant.
[c] TOF: the turnover frequency, the moles of 4-NP reduced per mole of Pt (or Au) per second.

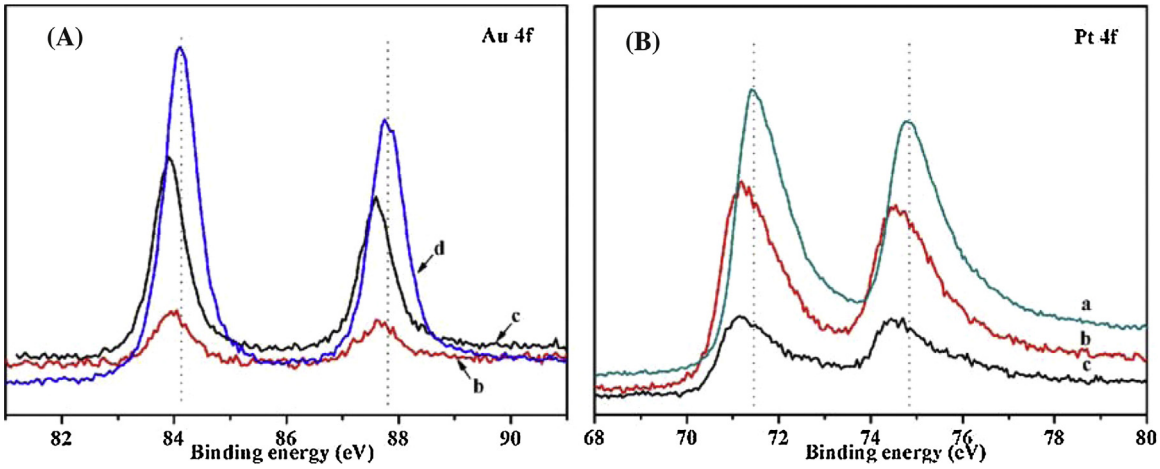

Fig. 3. XPS spectra of Au 4f (A) and Pt 4f (B) for different samples: (a) Pt-PDA/RGO, (b) Pt3Au1-PDA/RGO, (c) Pt1Au1-PDA/RGO, and (d) Au- PDA/RGO.

be attributed to the overlap between the absorption peak of RGO (at about 270 nm, in Fig. S3) and the peak of 4-AP. To further understand the influence of the absorption peak of RGO, we filtered the catalyst (Pt-Au-PDA/RGO) through a 0.22-μm nylon membrane filter before the UV–vis test. The time-dependent absorption spectra (Fig. S9) showed a successive intensity decrease of the absorption peak of 4-NP and a successive intensity increase of the absorption peak of 4-AP.

The effect of the support material on the catalytic performance was also studied. Fig. S7 shows the UV–vis absorption spectra of 4-NP with the reaction time in the presence of the Pt-PDA/RGO (a), Pt-RGO (b), and commercial Pt/C catalysts (c). Notably, the Pt-PDA/RGO catalyst exhibited the highest catalytic activity within 12 min to almost finish the reaction, whereas the Pt-RGO catalyst exhibited a significantly lower catalytic activity. On the other hand, the commercial Pt/C catalyst exhibited the lowest catalytic efficiency, which cannot achieve the full reduction of 4-NP even at a reaction time of 70 min. To reflect their catalytic efficiencies, the apparent rate constants (k_{app}) were calculated. This reaction is well known to follow pseudo-first order kinetics toward the concentration of 4-NP for the used excess $NaBH_4$. A good linear relationship of $-\ln(A)$ versus the reaction time t was observed for all catalysts (Fig. 4), confirming pseudo-first-order kinetics. The A value represents the absorbance at 400 nm, corresponding to different times. k_{app} could be determined from the slopes of $-\ln(A)$ vs. t plots. The k_{app} values shown in Fig. 4 and Table 1 demonstrate that the catalytic activity of the Pt catalysts supported on different supports decreases in the following order: Pt-PDA/RGO > Pt-RGO > Pt/C. The turnover frequency (TOF) is one important indicator to access catalytic activity, which was obtained by dividing the concentration of the raw material (4-NP) with the amount of the loading metal nanoparticles and reaction time [42,43]. Table 1 summarizes the

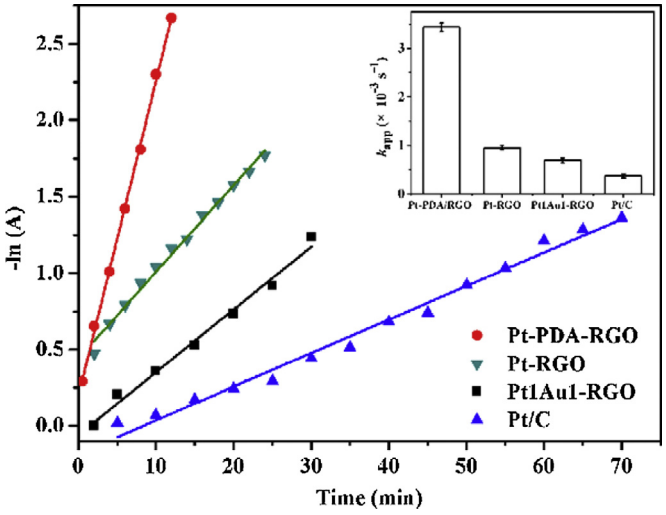

Fig. 4. Plots of the natural logarithm of the absorbance at 400 nm vs. the reduction time using Pt- PDA/RGO, Pt-RGO, Pt1Au1-RGO, and Pt/C as the catalysts. Inset: error bars represent the standard deviations of three measurements for each sample.

TOF values. Obviously, the TOF value of Pt-PDA/RGO was as high as almost 4 and 9 times of those for the Pt-RGO and Pt/C catalysts, respectively. The large difference in the catalytic activity is mainly attributed to the synergistic effect between Pt nanoparticles and graphene and good dispersivity of functionalized RGO. Compared with carbon black, due to the rich π structure of 4-NP, 4-NP can be adsorbed onto graphene via π–π stacking interactions [44], which will lead to a higher concentration of 4-NP near to the metal nanoparticles modified on graphene, thus exhibiting higher effi-

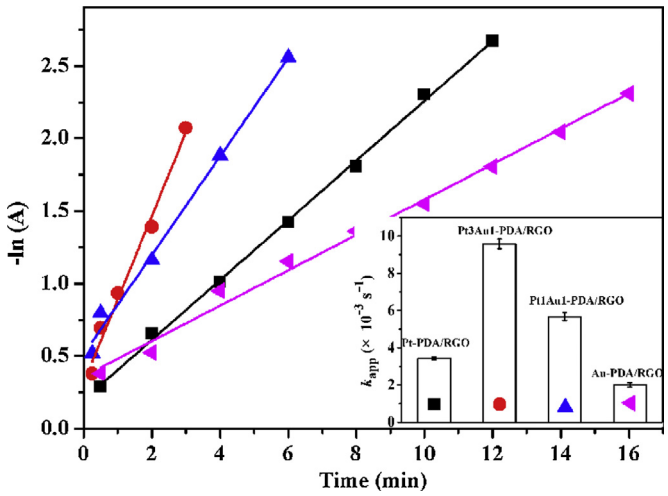

Fig. 5. Plots of the natural logarithm of the absorbance at 400 nm vs. the reduction time. Inset: error bars represent the standard deviations of three measurements for each sample.

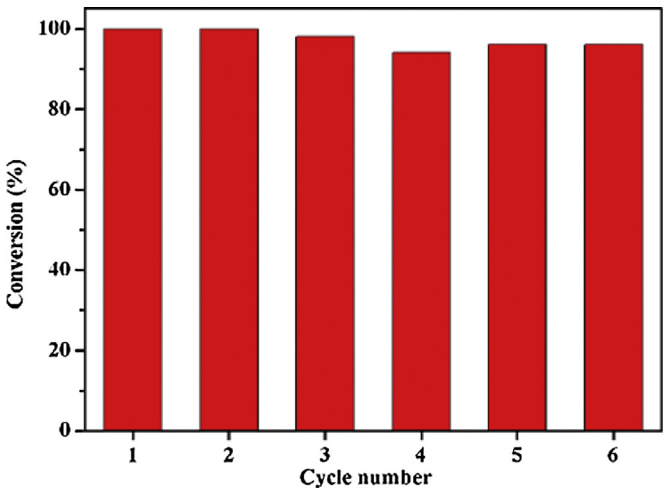

Fig. 6. Reusability of Pt3Au1-PDA/RGO as the catalyst for the reduction of 4-NP in six successive cycles.

ciency. Compared to that of pure RGO support, PDA-functionalized graphene exhibited good dispersivity in water [28,29], resulting in superior catalytic activity.

3.3. Effect of the chemical composition on catalytic activity

The effect of the chemical composition of the Pt–Au-PDA/RGO hybrids was also investigated. Fig. S8 shows the evolution of the absorbance data of the reduction of 4-NP over the Pt–Au-PDA/RGO hybrids with different molar ratios. From the plots of $-\ln(A)$ vs. t (Fig. 5), the k_{app} and TOF values were calculated, and Table 1 lists these values. The pure Pt-PDA/RGO sample exhibited a catalytic efficiency higher than that of the pure Au-PDA/RGO sample (72 vs. 42 h^{-1} of TOF). Besides, from Table 1, the Pt3Au1-PDA/RGO sample exhibited the highest reaction rate (9.58×10^{-3} s^{-1}) and TOF value. The values are approximately 2 and 4 times as compared to those for monometallic Pt-PDA/RGO and monometallic Au- PDA/RGO, respectively. For Pt–Au alloys, as the Pt content decreased, the reaction rate constants decreased. These observations indicate that the reaction rate for the reduction of 4-NP by $NaBH_4$ can be significantly improved as the Pt–Au alloy is formed at appropriate molar ratios.

As described previously [41,45], electron transfer from BH_4^- to 4-NP takes place only when both the species are adsorbed on the surface of the catalyst. Also, 4-NP prefers to adsorb on Au while BH_4^- is more likely to adsorb on Pt. Moreover, previous work indicates that excess electrons on Au atoms can transfer to the adjacent Pt atoms in a AuPt alloy [36]. Thereby, the reaction mechanism for the reduction of 4-NP with $NaBH_4$ based on the synergistic catalysis between Au and Pt is proposed as follows: (1) the significant enhancement of the electron density on Au and Pt atoms from the PDA coating can lead to improvement of the activity to target products, that is, 4-nitrophenolate and BH_4^- adsorb to neighboring Au and Pt atoms (respectively) at the surface of the Pt–Au alloy; (2) due to electron transfer from Au to Pt, electron enrichment onto the Pt atoms will facilitate the electron transfer from the adsorbed BH_4^- to 4- nitrophenolate adsorbed nearby on the Au. Such an electron transfer in Pt–Au alloy could be found in other work. For example, Zhang et al. [12] observed a similar higher reaction rate for the reduction of 4-NP by Pt–Au alloy nanoparticles/CeO_2 nanotubes as compared with those observed for the catalysis by pure Au and Pt samples, which originates from the electronic effect in Pt–Au alloy nanoparticles. Furthermore, the catalytic activities of Pt-RGO and Pt1Au1-RGO were compared; the latter was found to demonstrate lower activity (Fig. 4 and Table 1). Obviously, the two components did not interact owing to the phase-segregation state of Pt and Au from the XRD result (Fig. S4).

The normalized rate constant (k_{nor}) is a key indicator for estimating catalytic activity, which is associated with the amount of catalyst, *i.e.*, $k_{nor} = k_{app}/m$. Compared with other catalysts reported in the literature (Table S1), including Pt- [11,46,47], Ag- [48] and Au-based [43,49] catalysts, Pt3Au1-PDA/RGO exhibited a significantly higher k_{nor} value (1700 s^{-1} g^{-1}), strongly indicating the superior catalytic activity of Pt3Au1-PDA/RGO.

To investigate reusability, the Pt3Au1-PDA/RGO composite with the highest catalytic activity was used in the catalytic reduction of 4-NP, over six cycles. As shown in Fig. 6, the catalyst could be successfully recycled and reused for at least six successive cycles of the reaction, with a stable conversion efficiency of around 100%, indicating the good stability of the Pt–Au alloy nanoparticles in aqueous solutions.

3.4. Purification of 4-NP-contaminated water

Fang and Wang [50] have set up an experimental device of "filtering and catalyzing" for the purification of water containing nitro compounds. Here, we set up another device of "filtering and catalyzing." In Fig. S10, 30 mL of water containing 0.1 mM 4-NP and $NaBH_4$ in a beaker was stirred at 800 rpm. Then, 0.3 mL of Pt3Au1-PDA/RGO (3 mg/mL) was rapidly added in the beaker. After several seconds, the mixture was rapidly filtered using a decompress filter by using a vacuum pump. In only 2 s, the purified water exhibited a pale yellow. Furthermore, after 8 s, the water was colorless, and the peak at 400 nm was absent. This indicates the highly efficient degradation of 4-NP and the superior convenience of handling the as-prepared Pt–Au alloy nanoparticles-PDA/RGO.

4. Conclusions

A facile, green synthesis route toward highly active Pt–Au dendrimer-like alloy nanoparticles supported on PDA-functionalized RGO is demonstrated. The catalytic activity toward 4-NP reduction is found to depend on the support material and chemical composition. With Pt-to-Au ratios of 3/1 and 1/1, significantly enhanced activities for the Pt–Au-PDA/RGO samples were obtained in comparison to those obtained for the support decorated with monometallic Pt or Au nanoparticles, which is attributed to electronic transfers from the PDA coating to both Au

and Pt sites and from adjacent Au atoms to catalytically active Pt sites. Pt–Au dendrimer-like alloy nanoparticles-PDA/RGO samples exhibited superior catalytic stability and efficiency for purifying water containing 4-NP. It is believed that the as-prepared Pt–Au bimetallic nanoparticles-PDA/RGO will be used as a promising catalyst for applications in the degradation of organic compounds, caused by the easy and green synthesis and excellent catalytic activity.

Acknowledgment

This work is supported by the Fundamental Research Fund for the Central Universities (No. lzujbky-2014-69) and the Post-Doctoral Science Foundation of China (No. 2013M542393).

Appendix A. Supplementary data

Supplementary data associated with this article can be found, in the online version, at http://dx.doi.org/10.1016/j.apcatb.2015.08.013

References

[1] N. Li, P. Zhao, D. Astruc, Anisotropic gold nanoparticles: synthesis, properties, applications, and toxicity, Angew. Chem. Int. Ed. 53 (2014) 1756–1789.
[2] X. Sun, D. Li, Y. Ding, W. Zhu, S. Guo, Z.L. Wang, S. Sun, Core/shell Au/CuPt nanoparticles and their dual electrocatalysis for both reduction and oxidation reactions, J. Am. Chem. Soc. 136 (2014) 5745–5749.
[3] W. Lu, R. Ning, X. Qin, Y. Zhang, G. Chang, S. Liu, Y. Luo, X. Sun, Synthesis of Au nanoparticles decorated graphene oxide nanosheets: noncovalent functionalization by TWEEN 20 in situ reduction of aqueous chloroaurate ions for hydrazine detection and catalytic reduction of 4- nitrophenol, J. Harzard. Mater. 197 (2011) 320–326.
[4] G. Chang, Y. Luo, W. Lu, X. Qin, A.M. Asiri, A.O. Al-Youbi, X. Sun, Ag nanoparticles decorated polyaniline nanofibers: synthesis, characterization, and applications toward catalytic reduction of 4-nitrophenol and electrochemical detection of H_2O_2 and glucose, Catal. Sci. Technol. 2 (2012) 800–806.
[5] Z. Dong, X. Le, C. Dong, W. Zhang, X. Li, J. Ma, Ni@Pd core–shell nanoparticles modified fibrous silica nanospheres as highly efficient and recoverable catalyst for reduction of 4-nitrophenol and hydrodechlorination of 4-chlorophenol, Appl. Catal. B Environ. 162 (2015) 372–380.
[6] C. Mihut, C. Descorme, D. Duprez, M.D. Amiridis, Kinetic and spectroscopic characterization of cluster-derived supported Pt–Au catalysts, J. Catal. 212 (2002) 125–135.
[7] Y. Liu, B. Liu, Y. Liu, Q. Wang, W. Hu, P. Jing, L. Liu, S. Yu, J. Zhang, Improvement of catalytic performance of preferential oxidation of CO in H_2-rich gases on three-dimensionally ordered macro- and meso-porous Pt–Au/CeO_2 catalysts, Appl. Catal. B Environ. 142–143 (2013) 615–625.
[8] C. Xu, Y. Du, C. Li, J. Yang, G. Yang, Insight into effect of acid/base nature of supports on selectivity of glycerol oxidation over supported Au–Pt bimetallic catalysts, Appl. Catal. B Environ. 164 (2015) 334–343.
[9] N. Pradhan, A. Pal, T. Pal, Catalytic reduction of aromatic nitro compounds by coinage metal nanoparticles, Langmuir 17 (2001) 1800–1802.
[10] N. Pradhan, A. Pal, T. Pal, Silver nanoparticle catalyzed reduction of aromatic nitro compounds, Colloid Surf. A Physicochem. Eng. Asp. 196 (2002) 247–257.
[11] J. Lv, A. Wang, X. Ma, R. Xiang, J. Chen, J. Feng, One-pot synthesis of porous Pt–Au nanodendrites supported on reduced graphene oxide nanosheets toward catalytic reduction of 4-nitrophenol, J. Mater. Chem. A 3 (2015) 290–296.
[12] J. Zhang, G. Chen, D. Guay, M. Chaker, D. Ma, Highly active PtAu alloy nanoparticle catalysts for the reduction of 4-nitrophenol, Nanoscale 6 (2014) 2125–2131.
[13] A. Ma, J. Xu, X. Zhang, B. Zhang, D. Wang, H. Xu, Interfacial nanodroplets guided construction of hierarchical Au, Au–Pt, and Au–Pd particles as excellent catalysts, Sci. Rep. 4 (2014) 4849.
[14] L. Chen, L. Kuai, X. Yu, W. Li, B. Geng, Advanced catalytic performance of Au–Pt double-walled nanotubes and their fabrication through galvanic replacement reaction, Chem. -Eur. J. 19 (2013) 11753–11758.
[15] V.K. Gupta, S. Agarwal, T.A. Saleh, Synthesis and characterization of alumina-coated carbon nanotubes and their application for lead removal, J. Hazard. Mater. 185 (2011) 17–23.
[16] H. Khani, M.K. Rofouei, P. Arab, V.K. Gupta, Z. Vafaei, Multi-walled carbon nanotubes-ionic liquid-carbon paste electrode as a super selectivity sensor: application to potentiometric monitoring of mercury ion(II), J. Hazard. Mater. 183 (2010) 402–409.
[17] H. Wang, L. Thia, N. Li, X. Ge, Z. Liu, X. Wang, Selective electro-oxidation of glycerol over Au supported on extended poly(4-vinylpyridine) functionalized graphene, Appl. Catal. B Environ. 166–167 (2015) 25–31.
[18] S. Guo, S. Dong, E. Wang, Three- dimensional Pt-on-Pd bimetallic nanodendrites supported on graphene nanosheet: facile synthesis and used as an advanced nanoelectrocatalyst for methanol oxidation, ACS Nano 4 (2010) 547–555.
[19] Y. Zhang, Y. Gu, S. Lin, J. Wei, Z. Wang, C. Wang, Y. Du, W. Ye, One-step synthesis of PtPdAu ternary alloy nanoparticles on graphene with superior methanol electrooxidation activity, Electrochim. Acta 56 (2011) 8746–8751.
[20] H. Lee, S.M. Dellatore, W.M. Miller, P.B. Messersmith, Mussel-inspired surface chemistry for multifunctional coatings, Science 318 (2007) 426–430.
[21] B. Fei, B. Qian, Z. Yang, R. Wang, W.C. Liu, C.L. Mak, J.H. Xin, Coating carbon nanotubes by spontaneous oxidative polymerization of dopamine, Carbon 46 (2008) 1795–1797.
[22] W. Ye, D. Wang, H. Zhang, F. Zhou, W. Liu, Electrochemical growth of flowerlike gold nanoparticles on polydopamine modified ITO glass for SERS application, Electrochim. Acta 55 (2010) 2004–2009.
[23] L.Q. Xu, W.J. Yang, K.G. Neoh, E.T. Kang, G.D. Fu, Dopamine- induced reduction and functionalization of graphene oxide nanosheets, Macromolecules 43 (2010) 8336–8339.
[24] Y. Li, Z. Wang, X. Liu, S. Yang, H. Wang, J. Ou, Z. Li, J. Wang, A simple and feasible in-situ reduction route for preparation of graphene lubricant films applied to a variety of substrates, J. Mater. Chem. 22 (2012) 8036–8042.
[25] Z. Zhang, J. Zhng, B. Zhang, J. Tang, Mussel-inspired functionalization of graphene for synthesizing Ag-polydopamine-graphene nanosheets as antibacterial materials, Nanoscale 5 (2013) 118–123.
[26] Y. Fu, P. Li, Q. Xie, X. Xu, L. Lei, C. Chen, C. Zhou, W. Deng, S. Yao, One-pot preparation of polymer-enzyme-metallic nanoparticle composite films for high- performance biosensing of glucose and galactose, Adv. Funct. Mater. 19 (2009) 1784–1791.
[27] L. Guo, Q. Liu, G. Li, J. Shi, J. Liu, T. Wang, G. Jiang, A mussel- inspired polydopamine coating as a versatile platform for the in situ synthesis of graphene-based nanocomposites, Nanoscale 4 (2012) 5864–5867.
[28] W. Ye, Y. Chen, Y. Zhou, J. Fu, W. Wu, D. Gao, F. Zhou, C. Wang, D. Xue, Enhancing the catalytic activity of flowerike Pt nanocrystals using polydopamine functionalized graphene supports for methanol electrooxidation, Electrochim. Acta 142 (2014) 18–24.
[29] W. Ye, X. Shi, J. Su, Y. Chen, J. Fu, X. Zhao, F. Zhou, C. Wang, D. Xue, One-step reduction and functionalization protocol to synthesize polydopamine wrapping Ag/graphene hybrid for efficient oxidation of hydroquinone to benzoquinone, Appl. Catal. B- Environ. 160–161 (2014) 400–407.
[30] L. Wang, Y. Yamauchi, Strategic Synthesis of trimetallic Au@Pd@Pt core-shell Nanoparticles from poly(vinylpyrrolidone)-based aqueous solution toward highly active electrocatalysts, Chem. Mater. 23 (2011) 2457–2465.
[31] M.R. Knecht, M.G. Weir, A.I. Frenkel, R.M. Crooks, Structural rearrangement of bimetallic alloy PdAu nanoparticles within dendrimer templates to yield core/shell configurations, Chem. Mater. 20 (2008) 1019–1028.
[32] L. Vegard, The constitution of the mixed crystals and the filling of space of the atoms, Z. Fur Physik 5 (1921) 17–26.
[33] F. Xiao, F. Zhao, Y. Zhang, G. Guo, B. Zeng, Ultrasonic electrodeposition of gold–platinum alloy nanoparticles on ionic liquid-chitosan composite film and their application in fabricating nonenzyme hydrogen peroxide sensors, J. Phys. Chem. C 113 (2009) 849–855.
[34] B.N. Wanjala, J. Luo, B. Fang, D. Mott, C. Zhong, Gold–platinum nanoparticles: alloying and phase segregation, J. Mater. Chem. 21 (2011) 4012–4020.
[35] G. Zhang, B. Xu, Surprisingly strong effect of stabilizer on the properties of Au nanoparticles and Pt boolean and Au nanostructures in electrocatalysis, Nanoscale 2 (2010) 2798–2804.
[36] D. Tongsakul, S. Nishimura, K. Ebitani, Platinum/gold alloy nanoparticles-supported hydrotalcite catalyst for selective aerobic oxidation of polyols in base-free aqueous solution at room temperature, ACS Catal. 3 (2013) 2199–2207.
[37] C. Wang, W. Tian, Y. Ding, Y. Ma, Z.L. Wang, N.M. Markovic, V.R. Stamenkovic, H. Daimon, S. Sun, Rational synthesis of heterostructured nanoparticles with morphology control, J. Am. Chem. Soc. 132 (2010) 6524–6529.
[38] B. Baruah, G.J. Gabriel, M.J. Akbashev, M.E. Booher, Facile synthesis of silver nanoparticles stabilized by cationic polynorbornenes and their catalytic activity in 4-nitrophenol reduction, Langmuir 29 (2013) 4225–4234.
[39] S. Praharaj, S. Nath, S.K. Ghosh, S. Kundu, T. Pal, Immobilization and recovery of Au nanoparticles from anion exchange resin: resin-bound nanoparticle matrix as a catalyst for the reduction of 4-nitrophenol, Langmuir 20 (2004) 9889–9892.
[40] Y. Mei, Y. Lu, F. Polzer, M. Ballauff, Catalytic activity of palladium nanoparticles encapsulated in spherical polyelectrolyte brushes and core–shell microgels, Chem. Mater. 19 (2007) 1062–1069.
[41] C. Chu, Z. Su, Facile synthesis of AuPt alloy nanoparticles in polyelectrolyte multilayers with enhanced catalytic activity for reduction of 4-nitrophenol, Langmuir 30 (2014) 15345–15350.
[42] J. Hu, Y. Dong, X. Chen, H. Zhang, J. Zheng, Q. Wang, X. Chen, A highly efficient catalyst: *in situ* growth of Au nanoparticles on graphene oxide–Fe_3O_4 nanocomposite support, Chem. Eng. J. 236 (2014) 1–8.
[43] J. Li, C. Liu, Y. Liu, Au/graphene hydrogel: synthesis, characterization and its use for catalytic reduction of 4-nitrophenol, J. Mater. Chem. 22 (2012) 8426–8430.
[44] Y. Zhang, S. liu, W. Lu, L. Wang, J. Tian, X. Sun, In situ green synthesis of Au nanostructures on graphene oxide and their application for catalytic reduction of 4- nitrophenol, Catal. Sci. Technol. 1 (2011) 1142–1144.

[45] Y. Lu, J.Y. Yuan, F. Polzer, M. Drechsler, J. Preussner, In situ growth of catalytic active AuPt bimetallic nanorods in thermoresponsive core–shell microgels, ACS Nano 4 (2010) 7078–7086.
[46] Y.-Y. Shen, Y. Sun, L.-N. Zhou, Y.-J. Li, E.S. Yeung, Synthesis of ultrathin PtPdBi nanowire and its enhanced catalytic activity towards *p*-nitrophenol reduction, J. Mater. Chem. A 2 (2014) 2977–2984.
[47] S.K. Ghosh, M. Mandal, S. Kundu, S. Nath, T. Pal, Bimetallic Pt–Ni nanoparticles can catalyze reduction of aromatic nitro compounds by sodium borohydride in aqueous solution, Appl. Catal. A Gen. 268 (2004) 61–66.
[48] K.S. Shin, Y.K. Cho, J.-Y. Choi, K. Kim, Facile synthesis of silver-deposited silanized magnetite nanoparticles and their application for catalytic reduction of nitrophenols, Appl. Catal. A Gen 413–414 (2012) 170–175.
[49] Q. An, M. Yu, Y. Zhang, W. Ma, J. Guo, C. Wang, Fe_3O_4@carbon microsphere supported Ag–Au bimetallic nanocrystals with the enhanced catalytic activity and selectivity for the reduction of nitroaromatic Compounds, J. Phys. Chem. C 116 (2012) 22432–22440.
[50] Y. Fang, E. Wang, Simple and direct synthesis of oxygenous carbon supported palladium nanoparticles with high catalytic activity, Nanoscale 5 (2013) 1843–1848.